Original Article

Analysis of amyloid and tau deposition in Alzheimer's disease using ^{11}C-Pittsburgh compound B and ^{18}F-THK 5351 positron emission tomography imaging

ABSTRACT

This study aims to determine the deposition of ^{11}C-Pittsburgh compound B (^{11}C-PiB) and ^{18}F-THK 5351 using a normal database of the optimal cut-off-points for standardized uptake value ratios (SUVRs) in Alzheimer's disease (AD) patients. Sixteen AD patients and 24 cognitively normal individuals were enrolled in this study. The optimal cutoff points for the SUVR from the normal database were used for quantitative analysis. P-mod software with the Automated Anatomical Labeling merged atlas was employed to generate automatic volumes of interest to identify different brain regions, and the SUVRs of AD patients were compared with those of the age-matched normal controls. The correlation between PiB and THK5351 deposition at matching brain regions was identified. The mean regional ^{11}C-PiB SUVRs of the AD patients were significantly higher than the healthy controls ($P < 0.05$). The ^{11}C-PiB SUVR cut-offs were 1.46–1.81, with sensitivity ranging from 81.25% to 93.75% and specificity of 100%. The mean SUVRs of ^{18}F-THK 5351 in various regions were also significantly higher in the AD patients than in the healthy controls ($P < 0.05$). The inferior temporal gyrus yielded an optimum SUVR cut-off-points of 1.5 with 80% sensitivity and 83.33% specificity. The correlation of PiB and THK5351 SUVR was reported at precuneus, parietal, and occipital brain areas, with spearman's rho of 0.67, 0.66, and 0.72, respectively. Our findings allow determination of the SUVRs of ^{11}C-PiB and ^{18}F-THK-5351 amyloid and tau positron emission tomography tracers for clinical use, according to the normal database of the optimal cut-off-points for SUVRs in AD patients.

Keywords: ^{11}C-Pittsburgh compound B, ^{18}F-THK 5351, Alzheimer's disease, positron emission tomography

INTRODUCTION

Alzheimer's disease (AD) is characterized by the accumulation of amyloid-β (Aβ) and hyperphosphorylated tau proteins, along with neurodegeneration and cognitive impairment.[1-3] In 2015, dementia was estimated to affect 46.8 million people worldwide, with AD being the most common type.[3] The prevalence rates of AD rise with age and increase markedly after the age of 65 years.[4] Hence, it is important to realize the problem of dementia among the elderly population, and better screening and prevention are matters of great concern.

Aβ is known to be a disease biomarker, while tau is a disease progression biomarker.[5] Several radiotracers with high affinity to Aβ plaques and tau proteins have been employed for human positron emission tomography (PET) imaging. One of these tracers, Pittsburgh compound-B (^{11}C-PiB), is characterized by abnormal accumulation in extracellular Aβ plaques.[2,6,7] Meanwhile, ^{18}F-labeled arylquinoline derivatives have recently been developed as candidates for tau PET radiotracers. ^{18}F-THK-5351 studies demonstrated

Chotipanich Chanisa, Nivorn Monchaya, Kunawudhi Anchisa, Promteangtrong Chetsadaporn, Jantarato Attapon

National Cyclotron and PET Centre, Chulabhorn Hospital, Chulabhorn Royal Academy, Bangkok, Thailand

Address for correspondence: Prof. Chotipanich Chanisa, National Cyclotron and PET Centre, Chulabhorn Hospital, Chulabhorn Royal Academy, 906 Kamphaeng Phet 6 Road, Talat Bang Khen, Lak Si, Bangkok 10210, Thailand.
E-mail: chanisa.cho@pccms.ac.th

Submitted: 24-Apr-2020, **Revised:** 29-Apr-2020, **Accepted:** 16-May-2020, **Published:** 08-Oct-2020

How to cite this article: Chanisa C, Monchaya N, Anchisa K, Chetsadaporn P, Attapon J. Analysis of amyloid and tau deposition in Alzheimer's disease using ^{11}C-Pittsburgh compound B and ^{18}F-THK 5351 positron emission tomography imaging. World J Nucl Med 2021;20:61-72.

Access this article online	
Website: www.wjnm.org	Quick Response Code
DOI: 10.4103/wjnm.WJNM_50_20	

increased tracer uptake at the sites of tau pathology in AD, in association with the clinical severity of dementia.[2,8]

PiB and THK-5351 PET are thus beneficial for the diagnosis of early or preclinical stage AD, as well as for predicting the risk of AD development in patients with mild cognitive impairment (MCI) and those with abnormal genetic mutations, leading to better treatment planning in these groups of patients.[9]

In AD patients, there is a correlation between Aβ plaques and tau protein accumulation. This correlation has been confirmed by many studies, with Aβ plaques not being the only type of protein related to AD development.[10]

Thus, PiB and Tau PET imaging can play important roles in AD diagnosis from the preclinical presentation stage, and they can help predict the risk of AD in patients with MCI and individuals with genetic abnormalities.[10] These tracers can allow the differentiation of AD from other types of dementia with similar symptoms, which is crucial for the future care of patients.[11]

Hence, this study aimed to investigate the use of ^{11}C-PiB and ^{18}F-THK-5351 for AD diagnosis, using a normal database of the optimal cutoff points for SUVRs in AD patients. We also identify the correlation between PiB and THK5351 deposition at matching brain regions.

MATERIALS AND METHODS

This study was approved by the Human Research Ethics Committee of our institute on September 27, 2019. Project code was 051/2562. Before the study, written informed consent was obtained from all participants for participation in the study of data for research and educational purposes.

Participants

Sixteen AD patients (4 men, 11 women; aged 45–79 years; mean age ± standard deviation [SD]: 60.69 ± 6.82 years) and 24 cognitively normal individuals (13 men, 11 women; aged 42–79 years; mean age: 59.67 ± 10.84 years) were enrolled in this study. The cognitively normal individuals were verified as such by neurologists and neuropsychiatrists. Cognitively normal criteria were defined as: (1) mini-mental state examination of 24 of higher or score of more than 25 on the Montreal Cognitive Assessment (2) Clinical Dementia Rating of 0, (3) preserved activities of daily living, (4) absence of significant levels of impairment in other cognitive domains, (5) no sign and symptom of MCI or dementia, and (6) not diagnosed with probable AD by using criteria from the National Institute on Aging - Alzheimer's Association workgroups. All participants had no concurrent underlying disease such as hypertension, dyslipidemia, diabetic mellitus, cardiovascular disease, pulmonary, or renal condition. No normal individuals had a history of psychological or neurological disease, psychotropic drug use, or cancer within the past 5 years. Magnetic resonance imaging (MRI) brain of each cognitively normal individuals showed no focal mass, acute infarction, intracranial hemorrhage, hydrocephalus, extra-axial collection, or brain herniation. The AD participants were assessed and diagnosed by clinicians by using criteria from the National Institute on Aging - Alzheimer's Association workgroups for probable AD.[12]

Procedures

All participants underwent amyloid PET with ^{11}C-PiB and tau PET with ^{18}F-THK 5351, using a Siemens/Biograph 16 scanner in three-dimensional (3D) mode. For each patient, the two scans were performed within 2 weeks. MRI was also performed on all participants.

^{11}C-PiB imaging procedure

All participants were scanned using a Siemens/Biograph 16 scanner in 3D mode. Dynamic imaging was performed immediately after intravenous injection of 555 MBq (15 mCi) of ^{11}C-PiB. Dynamic brain PET/computed tomography (CT) scanning was performed for 70 min, and brain CT images were also acquired for attenuation correction. The image acquisition used a matrix size of 168, zoom of 1, and a Gaussian filter with a full-width at half-maximum (FWHM) of 5.0. Images were reconstructed into 7 frames of 10 min per frame, using ordered subset expectation maximization (OSEM) with 4 iterations, 8 subsets, and a 4-mm pixel size. The iterative reconstruction images from 50 to 70 min were used for quantitative analysis.

^{18}F-THK 5351 imaging procedure

Dynamic imaging was performed immediately after intravenous injection of 185 MBq (5 mCi) of ^{18}F-THK 5351. Dynamic brain PET/CT scanning was performed for 90 min and brain CT images for attenuation correction were also acquired. The image acquisition used a matrix size of 168, zoom of 1, and a Gaussian filter with a FWHM of 5.0. Images were reconstructed into 4 frames of 20 min per frame using OSEM with 4 iterations, 8 subsets, and a 4-mm pixel size. The iterative reconstruction images from 40 to 60 min were used for quantitative analysis.

MRI acquisition

T1-weighted MRI was acquired in all participants for registration and delineation of the brain reference regions using PMOD Neuro tool (PMOD Technologies, Zürich,

Switzerland). Additional sequences of MRI such as diffuse weight images, fluid-attenuated inversion recovery, T2W were used for detecting of other underlying intracranial pathologies.

Data and statistical analysis

The PET imaging data were processed and analyzed using P-mod Neuro tool (PMOD Technologies). Both ^{11}C-PiB and ^{18}F-THK-5351 PET images were automatically co-registered within individuals using an automatic voxel of interest method. Both the ^{11}C-PiB and ^{18}F-THK-5351 PET images were automatically co-registered to individual T1-weighting MRI images. Then, the SUVRs of ^{11}C-PiB and ^{18}F-THK 5351 in various cortical regions were analyzed, using the cerebellum as a reference region. The eight ^{11}C-PiB regions included orbitofrontal, precuneus, parietal, anterior cingulate, posterior cingulate, superior parietal, lateral temporal, and occipital areas. The ^{18}F-THK-5351 regions were the anterior cingulate, brain stem, caudate nucleus, white matter, entorhinal cortex, frontal cortex, fusiform gyrus, hippocampus, inferior temporal cortex, lingual gyrus, middle temporal gyrus, occipital cortex, pallidum, parahippocampal gyrus, parietal cortex, posterior cingulate, precuneus, putamen, and thalamus.

Analysis of variance (ANOVA) and multiple unpaired Bonferroni tests were performed to assess the tracer uptake in various cortical regions. For the different brain regions, differences between SUVR values were evaluated using ANOVA and multiple unpaired Bonferroni tests ($P < 0.05$, 2-sided), with $P < 0.05$ being considered statistically significant. STATA software version 11 (StataCorp LLC, Texas, USA) and Microsoft Excel for Mac 2011 (Microsoft Office campus, Washington, USA) were used for the analysis of all statistical data and graphical presentations.

Box and whisker plots were constructed for the SUVRs of the healthy controls and AD subjects. This plot is a method for graphically depicting groups of data through their quartiles, and indicates the variability outside the upper and lower quartiles. The cutoff points of the SUVRs of each brain region for evaluation of the deposition of ^{11}C-PiB and ^{18}F-THK-5351 were estimated from these plots.

All data from the AD patients and cognitively normal controls were analyzed using receiver-operating characteristic (ROC) curves to test the performance of the radiotracers for differentiating between disease and disease-free groups, as well as to acquire the sensitivity and specificity of each SUVR cutoff point. DeLong's method with the confidence level set at 95 was used for calculating the standard errors from the ROC plot. Spearman's rank correlation coefficient and *P* value for AD group were calculated by Spearman's rank correlation for nonparametric measurement, using STATA software version 11. The correlation between PiB and THK5351 deposition at matching brain regions was identified by Spearman's rank correlation coefficient >0.5 with value of $P < 0.05$. The SUVR of correlated brain regions between 2 radiotracers was plotted by Microsoft excel 2011.

RESULTS

The details of AD patients are shown in Table 1.

Quantitative analysis of ^{11}C-Pittsburgh compound B

In the AD patients aged ≤60 years, the mean (±SD) ^{11}C-PiB SUVRs in the posterior cingulate, precuneus, anterior cingulate, orbitofrontal, lateral temporal, parietal, superior parietal, and occipital regions were 1.95 ± 0.32, 1.89 ± 0.50, 1.93 ± 0.35, 1.92 ± 0.30, 1.83 ± 0.39, 1.73 ± 0.51, 1.69 ± 0.53, and 1.58 ± 0.41, respectively. In addition, in the AD patients aged over 60 years, the mean (±SD) ^{11}C-PiB SUVRs in the posterior cingulate, precuneus, anterior cingulate, orbitofrontal, lateral temporal, parietal, superior parietal, and occipital regions were 2.21 ± 0.30, 2.15 ± 0.29, 2.08 ± 0.30, 1.99 ± 0.31, 1.95 ± 0.31, 1.99 ± 0.32, 1.99 ± 0.25, and 1.83 ± 0.29, respectively. The mean SUVRs of the AD patients in both age groups were significantly higher than those of the normal controls ($P < 0.05$). However, the SUVR values showed no statistically significant differences between the right and left-side brain regions ($P > 0.05$). The results are shown in Tables 2 and 3. Box and whisker plots demonstrating the scatter in the ^{11}C-PiB SUVRs and the outlier values between the AD patients and the cognitively normal controls are shown in Figure 1.

Table 1: Alzheimer's disease patients' details

Patients	Age at presentation	Neurological evaluation		Duration of disease (year)
		MMSE	MoCA	
PT1	61	19	NA	3
PT2	63	22	13	2
PT3	62	21	12	1
PT4	58	20	8	2
PT5	63	NA	10	6
PT6	76	6	NA	3
PT7	68	NA	20	2
PT8	70	11	3	5
PT9	69	NA	17	2
PT10	66	NA	23	1
PT11	67	19	13	2
PT12	69	NA	8	9
PT13	65	NA	15	1
PT14	52	NA	22	2
PT15	47	NA	19	2

MMSE: Mini-mental state examination; MoCA: Montreal cognitive assessment

Table 2: Mean ^{11}C-PiB standardized uptake value ratio of healthy controls and alzheimer's disease patients

	AD Age ≤60 years (*n*=7)	HC Age ≤60 years (*n*=13)	*P*	AD Age >60 years (*n*=9)	HC Age >60 years (*n*=11)	*P*
Orbitofrontal	1.92±0.30	1.20±0.11	<0.05	1.99±0.31	1.25±0.13	<0.05
Precuneus	1.89±0.50	1.17±0.07	<0.05	2.15±0.29	1.14±0.18	<0.05
Parietal	1.73±0.51	1.14±0.08	0.0005	1.99±0.32	1.08±0.18	<0.05
Anterior cingulate	1.93±0.35	1.31±0.08	<0.05	2.08±0.30	1.29±0.17	<0.05
Posterior cingulate	1.95±0.32	1.40±0.07	<0.05	2.21±0.30	1.38±0.22	<0.05
Superior parietal	1.69±0.53	1.06±0.11	0.0006	1.99±0.25	0.96±0.18	<0.05
Lateral temporal	1.83±0.39	1.12±0.07	<0.05	1.95±0.31	1.11±0.09	<0.05
Occipital	1.58±0.41	1.16±0.09	0.002	1.83±0.29	1.14±0.12	<0.05

AD: Alzheimer's disease; HC: Healthy controls

Table 3: Regional ^{11}C-PiB standardized uptake value ratios in healthy controls and Alzheimer's disease patients, with comparisons between right and left sides of the brain

Region of interest	HC (*n*=24)	AD patients (*n*=16)	*P*
Right orbitofrontal	1.23±0.13	1.95±0.04	>0.05
Left orbitofrontal	1.24±0.17	1.94±0.29	
Right precuneus	1.15±0.12	2.01±0.42	>0.05
Left precuneus	1.15±0.13	1.99±0.44	
Right parietal	1.10±0.14	1.87±0.41	>0.05
Left parietal	1.12±0.13	1.85±0.44	
Right anterior cingulate	1.33±0.15	1.99±0.41	>0.05
Left anterior cingulate	1.28±0.12	2.00±0.30	
Right posterior cingulate	1.41±0.15	2.02±0.31	>0.05
Left posterior cingulate	1.38±0.16	2.13±0.33	
Right superior parietal	0.99±0.15	1.83±0.42	>0.05
Left superior parietal	1.02±0.16	1.88±0.42	
Right lateral temporal	1.12±0.09	1.89±0.35	>0.05
Left lateral temporal	1.13±0.09	1.87±0.35	
Right occipital	1.15±0.11	1.70±0.40	>0.05
Left occipital	1.15±0.09	1.69±0.39	

AD: Alzheimer's disease; HC: Healthy controls

Quantitative analysis of ^{18}F-THK 5351

In the AD subjects aged ≤60 years, the mean (±SD) SUVRs of THK 5351 in the caudate nucleus, putamen, pallidum, brain stem, posterior cingulate, precuneus, middle temporal gyrus, occipital cortex and inferior temporal regions were 1.34 ± 0.44, 1.92 ± 0.37, 2.19 ± 0.60, 1.73 ± 0.16, 1.68 ± 0.24, 1.42 ± 0.27, 1.44 ± 0.18, 1.35 ± 0.17, and 1.60 ± 0.21, respectively. In the AD subjects aged over 60 years, the mean (±SD) THK 5351 SUVRs in the caudate nucleus, putamen, pallidum, brain stem, posterior cingulate, precuneus, middle temporal gyrus, occipital cortex, and inferior temporal regions were 1.49 ± 0.37, 2.18 ± 0.31, 2.53 ± 0.38, 1.71 ± 0.14, 1.69 ± 0.24, 1.47 ± 0.18, 1.61 ± 0.31, 1.42 ± 0.15, and 1.86 ± 0.32, respectively. The mean SUVRs of the AD patients were significantly higher than the normal controls ($P < 0.05$) in both age groups, especially in the inferior temporal, occipital cortex, and middle temporal gyrus areas. However, there were no statistically significant differences between the right and left-side brain regions ($P > 0.05$). The results are shown in Tables 4 and 5. Box and whisker plots demonstrating the scatter in ^{18}F-THK5351 SUVRs and the outlier values between the AD patients and the cognitively normal controls are shown in Figure 2.

Receiver operating characteristic curves

ROC curve analysis is shown in Figures 3 and 4. The areas under the curves (AUC) of the PiB patients were remarkably high in all observed regions, ranging from 0.93 to 0.99. The CIs indicating the accuracies of the cutoff points obtained using another subject group in a different study ranged from 0.82 to 1.00, as shown in Table 6. The sensitivities and specificities are shown in Table 7. The optimum cutoff point SUVR in each region revealed a high sensitivity of more than or equal to 80%.

The THK 5351 ROC curve analysis showed high AUC values from 0.71 to 0.87 for the fusiform gyrus, inferior temporal cortex, middle temporal gyrus, occipital cortex, parahippocampus, parietal cortex, posterior cingulate, and precuneus regions, with CIs of 0.5–0.99, as presented in Table 8. The SUVRs cutoff for each brain area are shown in Table 9. The inferior temporal gyrus, an important brain area for the preclinical evaluation of AD, yielded an optimum SUVR cutoff of 1.5 with 80% sensitivity and 83.33% specificity.

Correlation

The statistical analysis of spearman rank correlation was applied to demonstrate the degree of correlation between SUVR of PiB and THK5351 uptake at matching brain regions of AD group, which investigated in both radiotracers including precuneus, anterior cingulate, posterior cingulate, parietal, and occipital. The strong correlation degree was demonstrated between tau and amyloid deposition at occipital with Spearman's rho = 0.72, followed by the correlation between PiB uptake at occipital and THK 5351 uptake at parietal with Spearman's rho = 0.58. The Spearman's rank correlation rho between PiB accumulation

Table 4: Mean ^{18}F-THK-5351 standardized uptake value ratios of healthy controls and Alzheimer's disease patients

	AD Age ≤60 years (n=6)	HC Age ≤60 years (n=13)	P	AD Age >60 years (n=9)	HC Age >60 years (n=11)	P
Anterior cingulate	1.63±0.12	1.67±0.05	0.348	1.61±0.28	1.71±0.19	0.366
Brain stem	1.73±0.16	1.84±0.06	0.037	1.71±0.14	1.91±0.18	0.012
Caudate nucleus	1.34±0.44	1.98±0.18	0.0003	1.49±0.37	1.93±0.27	0.006
White matter	1.44±0.19	1.40±0.08	0.473	1.52±0.19	1.48±0.18	0.603
Entorhinal cortex	1.52±0.21	1.51±0.08	0.875	1.73±0.36	1.69±0.24	0.782
Frontal cortex	1.22±0.18	1.25±0.04	0.516	1.36±0.21	1.28±0.13	0.284
Fusiform gyrus	1.55±0.22	1.40±0.05	0.032	1.73±0.17	1.48±0.20	0.009
Hippocampus	1.84±0.38	2.01±0.11	0.147	1.85±0.31	2.14±0.22	0.030
Inferior temporal cortex	1.60±0.21	1.37±0.04	0.001	1.86±0.32	1.48±0.21	0.006
Lingual gyrus	1.26±0.22	1.20±0.06	0.415	1.33±0.14	1.22±0.14	0.084
Middle temporal gyrus	1.44±0.18	1.27±0.04	0.003	1.61±0.31	1.34±0.16	0.022
Occipital cortex	1.35±0.17	1.16±0.05	0.001	1.42±0.15	1.18±0.12	0.001
Pallidum	2.19±0.60	2.49±0.15	0.095	2.53±0.38	3.01±0.55	0.040
Parahippocampal gyrus	1.98±0.37	1.78±0.09	0.082	2.04±0.26	1.90±0.23	0.209
Parietal cortex	1.23±0.26	1.16±0.04	0.382	1.34±0.16	1.18±0.11	0.013
Posterior cingulate	1.68±0.24	1.45±0.06	0.004	1.69±0.24	1.49±0.15	0.038
Precuneus	1.42±0.27	1.26±0.03	0.045	1.47±0.18	1.26±0.11	0.006
Putamen	1.92±0.37	2.05±0.08	0.224	2.18±0.31	2.33±0.39	0.358
Thalamus	1.47±0.61	2.11±0.11	0.001	1.86±0.37	2.26±0.28	0.013

AD: Alzheimer's disease; HC: Healthy controls

at precuneus and THK5351 accumulation at precuneus and parietal was 0.67 and 0.70, respectively. The Spearman's rho correlation SUVR between PiB retention at parietal and THK 5351 retention at precuneus, parietal, and occipital was 0.59, 0.66, and 0.60, respectively. PiB retention at posterior cingulate gyrus and THK5351 retention at parietal were correlative at Spearman's rho = 0.58. All these analyzed Spearman's rank degrees (outlined above) demonstrated the $P < 0.05$. However, there was a weak correlation (Spearman's rho < 0.5) between PiB accumulation at anterior cingulate gyrus and THK5351 uptake at other matching brain regions. Plots of correlative brain regions are shown in Figure 5.

DISCUSSION

The characteristics of Aβ plaque and tau protein accumulation in AD patients are very important for the discrimination of elderly cognitive normal subjects from AD patients. According to the study of Rowe *et al*.[13] the prevalence of amyloid-positive cases in healthy older subjects increased from 18% in the seventh decade of age to 60% in those over 80 years. Therefore, the incidence of AD is known to increase with age, with age becoming the most important risk factor for the development of AD.[4,14] Measurements of amyloid deposition in brain regions (SUVR values) may therefore assist physicians in differentiating elderly cognitively normal individuals from AD patients. However, the appropriate SUVR cutoff points for each brain region should be carefully considered.

The PET tracers ^{11}C-PiB and ^{18}F-THK-5351 have great potential for reflecting the physiology of AD, as they can reveal elevated Aβ and tau protein deposition in different brain regions.[15] In this study, we evaluated the deposition of these proteins using quantitative PET with SUVR analysis, and our findings showed distinctly elevated ^{11}C-PiB deposition in the anterior and posterior cingulate in AD patients, with the SUVRs being significantly higher than in the normal controls [$P < 0.05$; Table 2]. These findings are compatible with those of Koivunen *et al*.[16] and Kemppainen *et al*.[17] where high Aβ accumulation was demonstrated in the anterior and posterior cingulate. The tracer deposits at these regions reflect the development of heavy Aβ loads in AD patients.[18]

We found high ^{18}F-THK-5351 deposition in the pallidum and putamen in the elderly cognitively normal individuals [Tables 4 and 5]. This finding is similar to that of the study of Lockhart *et al*.[19] which reported SUVRs of 3.58 and 2.94 for the pallidum and thalamus, respectively.[9] Furthermore, ^{18}F-THK-5351 also deposit in the inferior temporal cortex being significant region for preclinical AD.[20] Thus, ^{18}F-THK-5351 imaging is useful for the early detection of neurofibrillary pathology in AD patients. The study showed higher ^{18}F-THK-5351 SUVRs in AD subjects than in the elderly cognitively normal controls ($P < 0.05$). A similar finding was reported by Harada *et al*.,[8] with higher SUVR values in AD patients (three patients) 2.21 ± 0.24 than in healthy controls (mean 1.54 ± 0.12). The findings facilitated the differentiation of AD patients from cognitively normal subjects according to the deposition of ^{18}F-THK-5351 in the

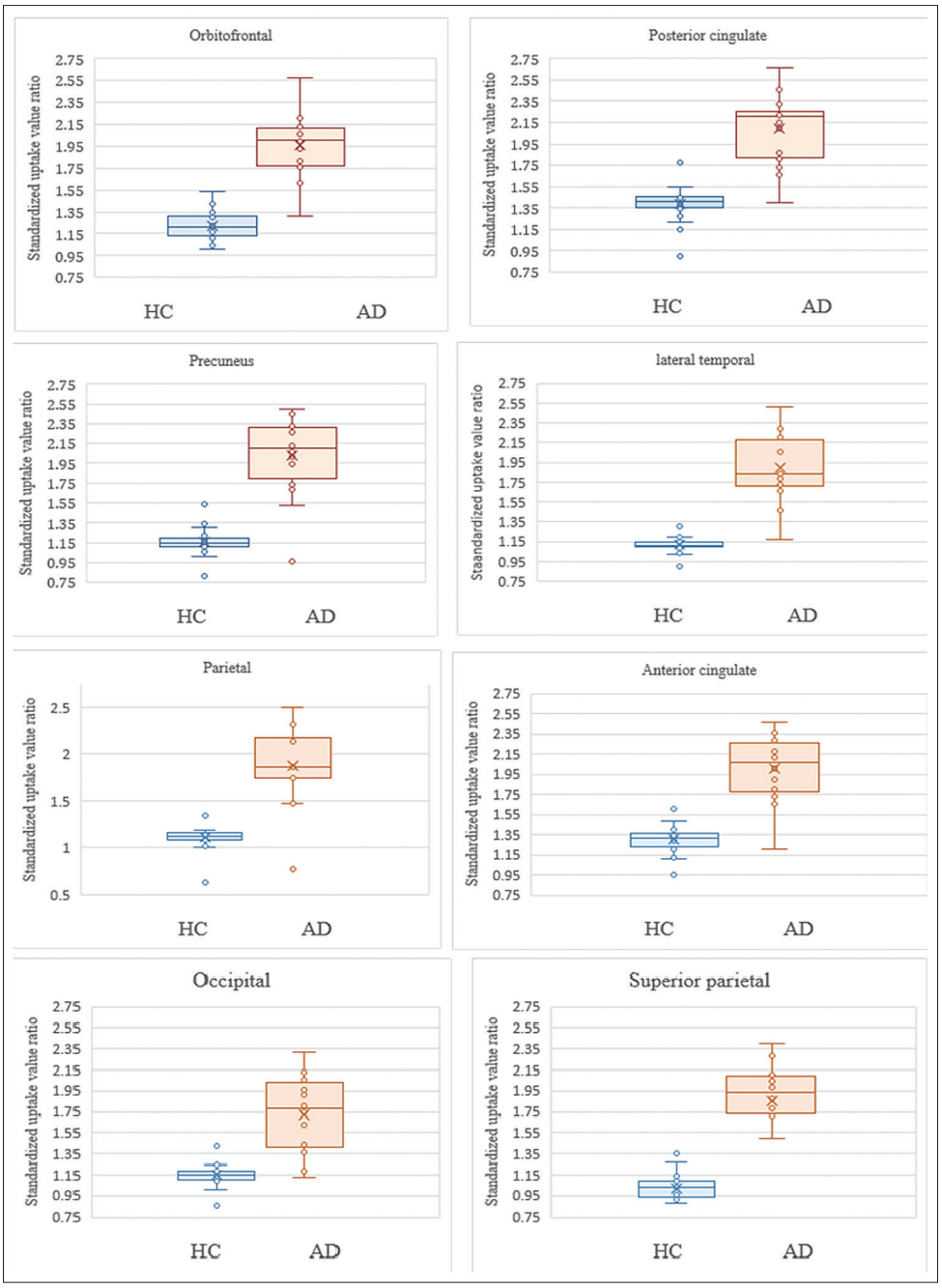

Figure 1: Box and whisker plots for various regions with comparison of the scatter of ^{11}C-PiB SUVRs and outlier values between the HC and AD groups. AD: Alzheimer's disease; HC: Healthy controls; ^{11}C-PiB: ^{11}C-Pittsburgh compound B; SUVRs: Standardized uptake value ratios

inferior temporal cortex. However, ^{18}F-THK-5351 is frequently present in the brains of cognitively normal older adults, not only AD patients. In addition, we observed that in the age groups over 60 years, the SUVR values for ^{18}F-THK-5351 were significantly higher in the elderly cognitively normal controls than in the AD patients in the caudate nucleus, palladium, and thalamus regions ($P < 0.05$). Our findings share some similarities with those of the study of Lockhart *et al*.[19] which found higher SUVR values in healthy controls than in AD patients in the brain stem, caudate nucleus, and hippocampus, although the differences were not statistically significant.

Notably, the ROC analysis showed that the ^{11}C-PiB cut-off for the average SUVR in each region yielded a high AUC for the discrimination between AD and non-AD subjects. For all regions, the SUVR cut-offs were approximately 1.46–1.81, with high sensitivity ranging from 81.25% to 93.75% and specificity of 100%, with a CI of 0.82–1.00. Previous studies by Ismail *et al*.,[21] Villeneuve *et al*.,[22] and Jack *et al*.[23] provided

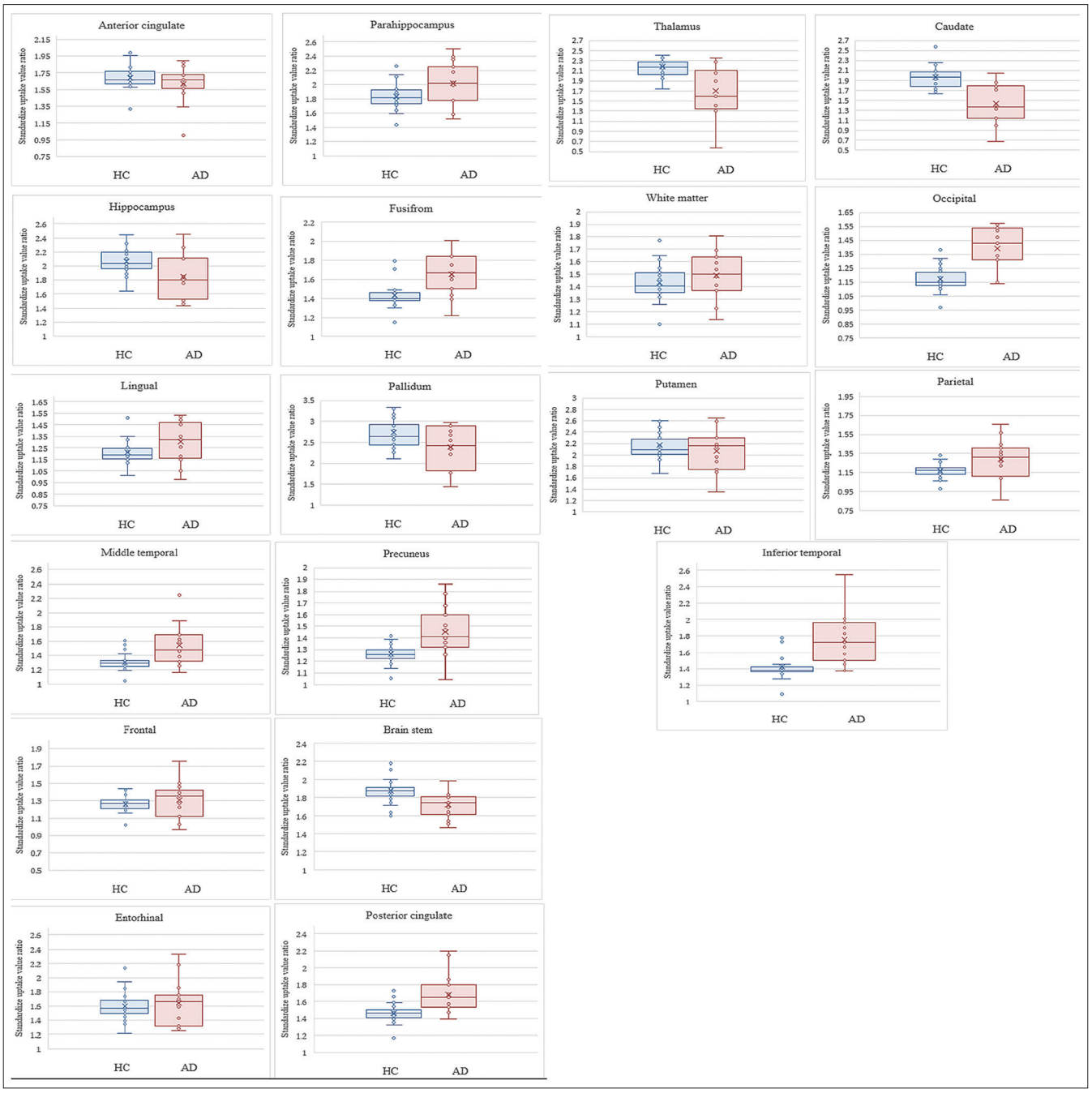

Figure 2: Box and whisker plots for various regions comparing the scatter of ^{18}F-THK5351 SUVRs and outlier values between HC and AD groups. AD: Alzheimer's disease; HC: Healthy controls; SUVRs: Standardized uptake value ratios

only average SUVRs for the global cortical region of 1.2–1.5, 1.21, and 1.42, respectively, without giving the sensitivity or specificity of particular SUVR cutoffs for a normal population. As mentioned, the cutoffs obtained from the ROC curve showed some differences between our study and previous ones. Nevertheless, our study did not focus on finding an average SUVR for multiple cortical regions like other studies, but instead focused on obtaining values for local regions, which we think may be a more precise and less complex method in clinical practice.

In our study, ^{11}C-PiB showed very high sensitivity and specificity in all regions. However, the ROC analysis of ^{18}F-THK5351 demonstrated some differences. The cut-off value analyzed from the ROC of tau phosphorylation retention was found to result in extremely low AUCs in most regions, resulting from their being little difference between the average SUVRs of AD individuals and healthy controls. Regions presenting with low AUCs and low differences, which correlated with off-target binding, were revealed in deep parts of the brain, including the caudate,

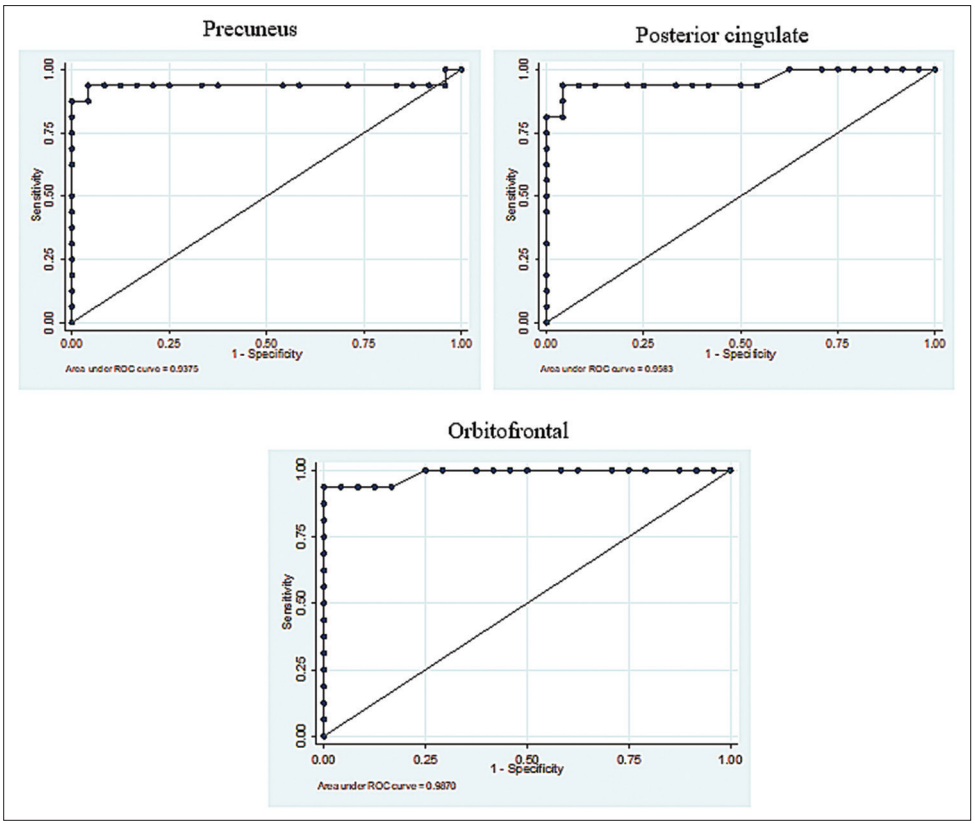

Figure 3: ^{11}C-PiB ROCs from the average SUVRs between elderly cognitively normal individuals and AD patients, with the ROCs indicating high AUCs, and the very high diagnostic performance of PiB in the precuneus, posterior cingulate, and orbitofrontal regions. ROCs: Receiver-operating characteristics; ^{11}C-PiB: ^{11}C-Pittsburgh compound B; SUVRs: Standardized uptake value ratios; AUCs: Areas under the curves

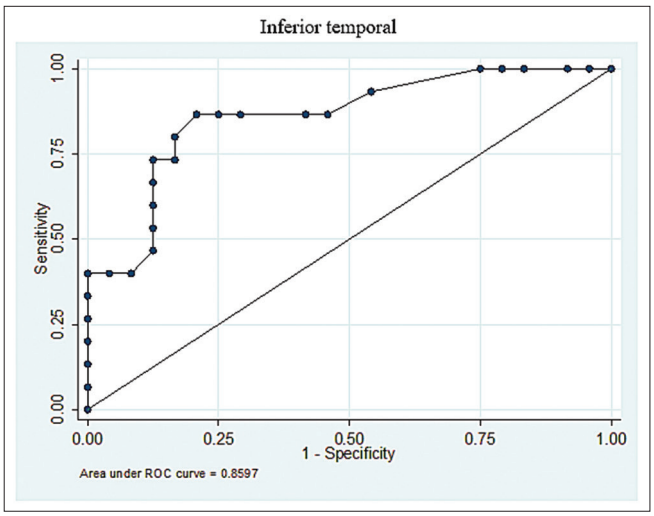

Figure 4: ^{18}F-THK5351 ROCs from the average SUVRs between elderly cognitively normal individuals and AD patients in the inferior temporal region, with the ROCs indicating noticeably high AUCs, and the very high performance of THK 5351 in the inferior temporal area for the differential diagnosis of AD. ROCs: Receiver-operating characteristics; AUCs: Areas under the curves; AD: Alzheimer's disease; SUVRs: Standardized uptake value ratios

thalamus, putamen, and pallidum.[24] The low differences found between the average SUVRs of both groups in the remaining areas, including the hippocampus, entorhinal, and frontal regions, may be impacted by misregistration for anatomical differences. For example, atrophy of a gyrus may cause misregistration because of anatomical differences, especially with the lack of a voxel-based morphology correction. Thus, the areas with a low SUVR difference between the disease and the disease-free subjects were linked to low AUCs and could be interpreted as ineffective regions for differential evaluation or screening of Alzheimer's patients. The regions with large differences in SUVR between AD and non-AD, as well as high AUCs, were the parahippocampus, fusiform, precuneus, middle temporal, parietal, and posterior cingulate regions, and especially the inferior temporal gyrus. The ROC analysis indicated an SUVR cut off for the inferior temporal region for preclinical screening of 1.5, with this having an 80% sensitivity, 83.33% specificity, and CI of 0.74–0.98. In the same manner as those studies concerned with ^{11}C-PiB, most previous studies on tau deposition also focused on the average SUVR or distribution volume ratio without describing the specific specificity and sensitivity of the cutoff, but some similarities can still be discussed.[8,20] The study shared the same value as the study of Lockhart *et al*.[20] which reported a mean SUVR for healthy controls (HC) of 1.5,

Table 5: Regional ^{18}F-THK 5351 standardized uptake value ratios in healthy controls and Alzheimer's disease patients with comparisons between right and left sides of the brain

Region of interest	HC (n=24)	AD patients (n=15)	P
Right anterior cingulate	1.67±0.15	1.65±0.17	0.75
Left anterior cingulate	1.71±0.12	1.70±0.14	0.93
Brain stem	1.87±0.13	1.72±0.14	1.16E-3
Right caudate nucleus	2.02±0.24	1.47±0.42	1.00E-5
Left caudate nucleus	1.90±0.26	1.39±0.38	2.00E-5
White matter	1.44±0.14	1.49±0.19	0.29
Right entorhinal cortex	1.61±0.22	1.65±0.33	0.65
Left entorhinal cortex	1.58±0.17	1.64±0.32	0.43
Right frontal cortex	1.26±0.09	1.29±0.19	0.47
Left frontal cortex	1.27±0.09	1.31±0.23	0.43
Right fusiform gyrus	1.43±0.14	1.65±0.23	4.70E-4
Left fusiform gyrus	1.44±0.16	1.65±0.22	1.18E-3
Right hippocampus	1.99±0.25	1.82±0.33	0.07
Left hippocampus	2.10±0.20	1.88±0.34	0.01
Right inferior temporal cortex	1.40±0.14	1.77±0.29	1.00E-5
Left inferior temporal cortex	1.45±0.17	1.73±0.35	1.38E-3
Right lingual gyrus	1.21±0.10	1.31±0.18	0.03
Left lingual gyrus	1.21±0.10	1.29±0.19	0.11
Right middle temporal gyrus	1.30±0.12	1.58±0.28	1.10E-4
Left middle temporal gyrus	1.31±0.12	1.51±0.29	4.86E-3
Right occipital cortex	1.17±0.09	1.40±0.16	7.00E-7
Left occipital cortex	1.17±0.09	1.38±0.17	9.00E-6
Right pallidum	2.71±0.47	2.40±0.46	0.06
Left pallidum	2.76±0.46	2.39±0.54	0.03
Right parahippocampal gyrus	1.85±0.18	2.06±0.36	0.02
Left parahippocampal gyrus	1.81±0.18	1.99±0.27	0.01
Right parietal cortex	1.17±0.08	1.31±0.20	3.88E-3
Left parietal cortex	1.17±0.08	1.28±0.21	0.03
Right posterior cingulate	1.46±0.12	1.68±0.23	1.91E-4
Left posterior cingulate	1.47±0.11	1.68±0.23	4.17E-4
Right precuneus	1.27±0.08	1.47±0.21	1.70E-4
Left precuneus	1.26±0.08	1.42±0.22	1.21E-3
Right putamen	2.11±0.28	2.05±0.34	0.55
Left putamen	2.25±0.33	2.09±0.37	0.16
Right thalamus	2.19±0.23	1.75±0.49	4.60E-4
Left thalamus	2.17±0.20	1.68±0.50	1.20E-4

AD: Alzheimer's disease; HC: Healthy controls

Table 6: Areas under the curves of ^{11}C-PiB

Region of interest	AUC	Confidence interval
Orbitofrontal	0.99	0.96-1.00
Precuneus	0.94	0.82-1.00
Parietal	0.94	0.82-1.00
Anterior cingulate	0.95	0.84-1.00
Posterior cingulate	0.96	0.89-1.00
Superior parietal	0.94	0.82-1.00
Lateral temporal	0.99	0.96-1.00
Occipital	0.93	0.84-1.00

whereas a study by Kikuchi *et al*.[25] reported a different SUVR of 1.56 ± 0.09 for the right middle inferior temporal region of HCs, and 1.52 ± 0.12 for the left middle inferior temporal region. Harada *et al*.[8] also presented inferior temporal SUVRs in HCs, with these ranging from 1.44 to 1.67.

Table 7: PiB standardized uptake value ratio s cut off for each brain area

Region of interest	SUVR cut-off	Sensitivity	Specificity
Orbitofrontal	1.61	93.75	100
Precuneus	1.68	87.5	100
Parietal	1.48	93.75	100
Anterior cingulate	1.66	93.75	100
Posterior cingulate	1.81	81.25	100
Superior parietal	1.5	93.75	100
Lateral temporal	1.46	93.75	100
Occipital	1.36	87.5	95.83

Selected optimum cut-offs at a sensitivity level ≥80% and the highest specificity level. SUVR: Standardized uptake value ratio

Table 8: Areas under the curves s of ^{18}F-THK 5351

Region of interest	AUC	CI
Anterior cingulate	0.43	0.22-0.64
Brain stem	0.18	0.04-0.32
Caudate nucleus	0.13	0.01-0.25
White matter	0.62	0.42-0.82
Entorhinal cortex	0.56	0.35-0.78
Frontal cortex	0.60	0.39-0.82
Fusiform gyrus	0.81	0.66-0.97
Hippocampus	0.28	0.08-0.49
Inferior temporal cortex	0.86	0.74-0.98
Lingual gyrus	0.67	0.48-0.88
Middle temporal gyrus	0.81	0.66-0.97
Occipital cortex	0.87	0.76-1.00
Pallidum	0.35	0.01-0.25
Parahippocampal gyrus	0.71	0.51-0.91
Parietal cortex	0.73	0.53-0.94
Posterior cingulate	0.83	0.65-0.96
Precuneus	0.84	0.69-0.99
Putamen	0.47	0.26-0.68
Thalamus	0.22	0.05-0.40

CI: Confidence interval; AUC: Areas under the curve

The quantitative results for both radiotracers not only demonstrated higher SUVR in various regions but also showed remarkable correlation between phosphorylated tau and amyloid deposition in AD group at matching brain regions, including occipital, parietal lobe, precuneus, and posterior cingulate gyrus. This was observed in our AD subjects diagnosed with advance stage of AD pathologies according to PET imaging and clinical presentation of dementia and in corresponding with the Braak[26] staging tau deposition and amyloid deposition staging, which presented the progression of amyloid and tau deposition in AD patients. The Braak staging for our patients was Braak stage V/VI, which represented the spreading of phosphorylated from the entorhinal cortex (Braak stages

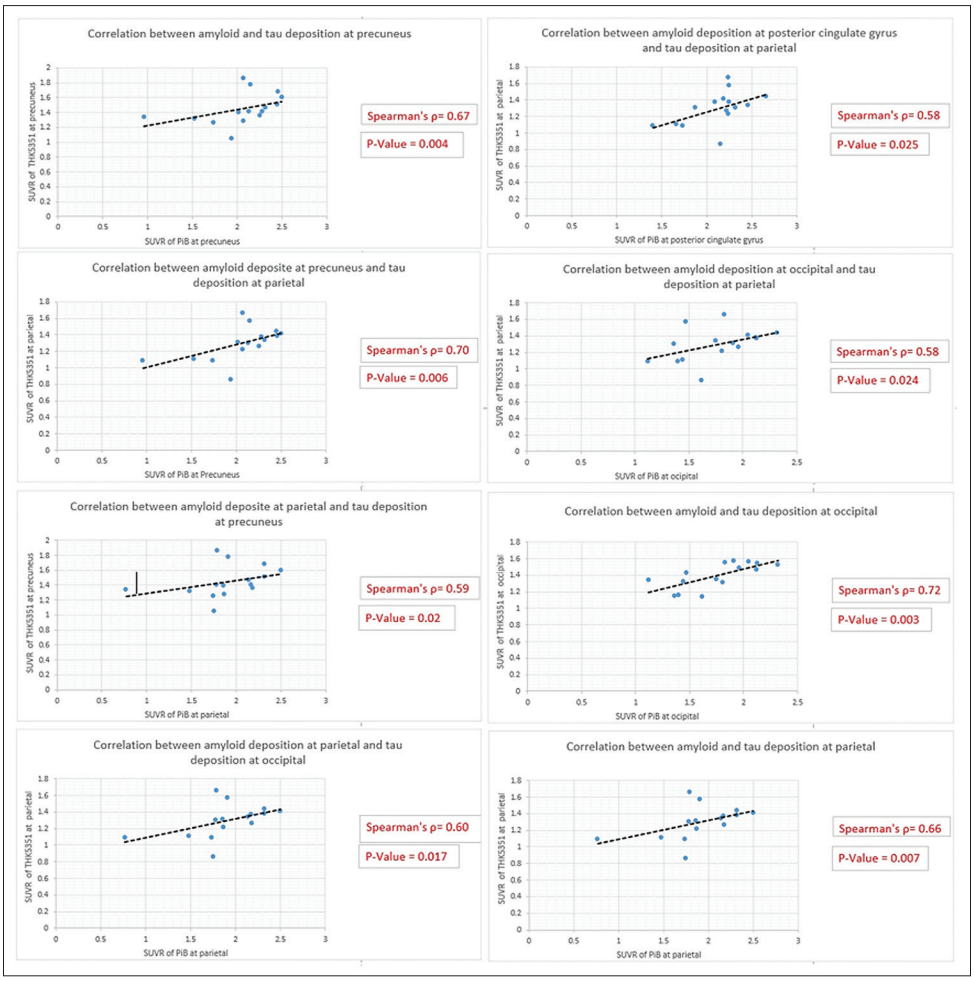

Figure 5: The SUVR correlation between THK 5351 and PiB in AD group. SUVR: Standardized uptake value ratio; PiB: Pittsburgh compound B; AD: Alzheimer's disease

I/II) to the inferolateral temporal cortex and parts of the medial parietal lobe (stages III/IV), then all-over neocortical cortex. Comparatively, Thal *et al*. reported the pattern of amyloid deposition that correlated to the clinical presentation, with the spreading of amyloid plaque from cortical cortex to area of cingulate gyrus and precuneus in phase 2/3 of dementia subjects, according to our results and clinical data of AD subjects.[27] Hence, the correlation of noticeably high SUVR between amyloid and tau deposition at occipital, parietal, precuneus, and posterior cingulate gyrus in our clinically proven AD subjects may related to the spreading of phosphorylated Tau and amyloid in the late stage of the disease. Moreover, the correlation could be applied as the indicator for verifying the accuracy of diagnosed AD subjects in our analysis.

In summary, for normal controls, we found an ^{18}F-THK 5351 SUVR cutoff of 1.5 in the inferior temporal region, with this having a sensitivity of 80% and specificity of 83.33%, which was lower than the average SUVRs of AD patients, which were 1.60 ± 0.21 and 1.86 ± 0.32 for age groups ≤60 years and over 60 years, respectively. In addition, the correlation between SUVR of PiB and THK5351 was demonstrated in the regions according to the Braak staging tau deposition and Thal amyloid deposit phase, which presented the pathology in clinical AD.

Evidently, it can be concluded that both the ^{11}C-PiB and ^{18}F-THK 5351 SUVR cut-offs found in this study were different from those in previous studies. Hence, we recommended the utilization of a local database with population-specific cutoffs, which should help to provide highly reliable quantitative analysis resulting in the highest accuracy and precision for interpretation.

Our study was limited by the small number of participants. A greater number of patients would improve the accuracy, sensitivity, and specificity of the cutoff thresholds. Furthermore, the SUVR calculated from P-mod software might be subject to variation in some subjects with noticeable brain atrophy, because of the lack of a voxel-based morphology correction. ^{18}F-THK 5351 tracer itself has limitations because

Table 9: THK 5351 standardized uptake value ratio s cut off for each brain area

Region of interest	SUVR cut off	Sensitivity	Specificity
Anterior cingulate	1.56	93.33	4.17
Brain stem	1.62	80	4.17
Caudate nucleus	1.67	40	4.17
White matter	1.37	80	25
Entorhinal cortex	1.25	100	4.17
Frontal cortex	1.03	93.33	4.17
Fusiform gyrus	1.5*	80	87.5
Hippocampus	1.75	66.67	4.17
Inferior temporal cortex	1.5*	80	83.33
Lingual gyrus	1.16	80	25
Middle temporal gyrus	1.31*	86.67	66.67
Occipital cortex	1.31*	80	87.5
Pallidum	2.21	73.33	4.17
Parahippocampal gyrus	1.78	80	29.17
Parietal cortex	1.11	80	16.67
Posterior cingulate	1.53*	80	79.17
Precuneus	1.32*	80	83.33
Putamen	1.75	80	4.17
Thalamus	1.9	46.67	4.17

*Selected optimum cut-offs at a sensitivity level ≥80% and the highest specificity level. SUVR: Standardized uptake value ratio

^{18}F-THK 5351 PET has off-target binding to monoamine oxidase-B (MAO-B).[28,29] The tracer is known to accumulate not only neurofibrillary tangles but neurofibrillary tangles combining with reactive astrocytes. MAO-B distribution throughout the whole brain and subcortical structure should be concerned for tau PET interpretation.

CONCLUSION

The study used a normal database to determine the optimal cutoff points for ^{11}C-PiB and ^{18}F-THK 5351 SUVRs for determining positive amyloid and tau PET status in AD patients. Moreover, the correlation between tau and amyloid deposition at the cortical region, precuneus, and posterior cingulate gyrus in AD patients accordance with Braak staging tau deposition and Thal amyloid deposit phase.

Financial support and sponsorship

Chulabhorn Hospital, Chulabhorn Royal Academy.

Conflicts of interest

There are no conflicts of interest.

REFERENCES

1. Betthauser TJ, Lao PJ, Murali D, Barnhart TE, Furumoto S, Okamura N, *et al*. *In vivo* comparison of tau radioligands 18 F-THK-5351 and 18 F-THK-5317. J Nucl Med 2017;58:996-1002.
2. Brier MR, Gordon B, Friedrichsen K, McCarthy J, Stern A, Christensen J, *et al*. Tau and Aβ imaging, CSF measures, and cognition in Alzheimer's disease. Sci Transl Med 2016;8:338ra66.
3. Barc K, Kuźma-Kozakiewicz M. Positron emission tomography neuroimaging in neurodegenerative diseases: Alzheimer's disease, Parkinson's disease, and amyotrophic lateral sclerosis. Neurol Neurochir Pol 2019;53:99-112.
4. Mayeux R, Stern Y. Epidemiology of Alzheimer disease. Cold Spring Harb Perspect Med 2012;2:a006239. doi: 10.1101/cshperspect.a006239.
5. Okamura N, Harada R, Furumoto S, Arai H, Yanai K, Kudo Y. Tau PET imaging in Alzheimer's disease. Curr Neurol Neurosci Rep 2014;14:500.
6. Mintun MA, Larossa GN, Sheline YI, Dence CS, Lee SY, Mach RH, *et al*. [11C]PIB in a nondemented population: Potential antecedent marker of Alzheimer disease. Neurology 2006;67:446-52.
7. Rabinovici GD, Furst AJ, O'Neil JP, Racine CA, Mormino EC, Baker SL, *et al*. 11C-PIB PET imaging in Alzheimer disease and frontotemporal lobar degeneration. Neurology 2007;68:1205-12.
8. Harada R, Okamura N, Furumoto S, Furukawa K, Ishiki A, Tomita N, *et al*. 18F THK 5351: A novel PET radiotracer for imaging neurofibrillary pathology in Alzheimer disease. J Nucl Med. 2016;57:208-14.
9. Wang YT, Edison P. Tau imaging in neurodegenerative diseases using positron emission tomography. Curr Neurol Neurosci Rep 2019;19:45.
10. Koychev I, Gunn RN, Firouzian A, Lawson J, Zamboni G, Ridha B, *et al*. PET Tau and amyloid-β burden in mild Alzheimer's Disease: Divergent relationship with age, cognition, and cerebrospinal fluid biomarkers. J Alzheimers Dis 2017;60:283-93.
11. Melis RJF, Haaksma ML, Muniz-Terrera G. Understanding and predicting the longitudinal course of dementia. Curr Opin Psychiatry 2019;32:123-9.
12. McKhann GM, Knopman DS, Chertkow H, Hyman BT, Jack CR Jr., Kawas CH. The diagnosis of dementia due to Alzheimer's disease: Recommendations from the national institute on aging-Alzheimer's association workgroups on diagnostic guidelines for Alzheimer's disease. Alzheimers Dement 2011;7:263-9.
13. Rowe CC, Ellis KA, Rimajova M, Bourgeat P, Pike KE, Jones G, *et al*. Amyloid imaging results from the Australian Imaging, Biomarkers and Lifestyle (AIBL) study of aging. Neurobiol Aging 2010;31:1275-83.
14. Guerreiro R, Bras J. The age factor in Alzheimer's disease. Genome Med 2015;7:106.
15. Hanseeuw BJ, Betensky RA, Jacobs HIL, Schultz AP, Sepulcre J, Becker JA, *et al*. Association of amyloid and tau with cognition in preclinical Alzheimer disease: A longitudinal study. JAMA Neurol 2019;76:915-24.
16. Koivunen J, Scheinin N, Virta JR, Aalto S, Vahlberg T, Någren K, *et al*. Amyloid PET imaging in patients with mild cognitive impairment: A 2-year follow-up study. Neurology 2011;76:1085-90.
17. Kemppainen NM, Aalto S, Wilson IA, Någren K, Helin S, Brück A, *et al*. PET amyloid ligand [11C]PIB uptake is increased in mild cognitive impairment. Neurology 2007;68:1603-6.
18. Chételat G, La Joie R, Villain N, Perrotin A, de La Sayette V, Eustache F, *et al*. Amyloid imaging in cognitively normal individuals, at-risk populations and preclinical Alzheimer's disease. Neuroimage Clin 2013;2:356-65.
19. Lockhart SN, Baker SL, Okamura N, Furukawa K, Ishiki A, Furumoto S, *et al*. Dynamic PET measures of tau accumulation in cognitively normal older adults and Alzheimer's disease patients measured using [18F] THK-5351. PLoS One 2016;11:e0158460.
20. Sone D, Imabayashi E, Maikusa N, Okamura N, Furumoto S, Kudo Y, *et al*. Regional tau deposition and subregion atrophy of medial temporal structures in early Alzheimer's disease: A combined positron emission tomography/magnetic resonance imaging study. Alzheimers Dement (Amst) 2017;9:35-40.
21. Ismail R, Parbo P, Hansen KV, Schaldemose JL, Dalby RB, Tietze A,

et al. Abnormal amyloid load in mild cognitive impairment: The effect of reducing the PiB-PET Threshold. J Neuroimaging 2019;29:499-505.
22. Villeneuve S, Rabinovici GD, Cohn-Sheehy BI, Madison C, Ayakta N, Ghosh PM, *et al*. Existing Pittsburgh Compound-B positron emission tomography thresholds are too high: Statistical and pathological evaluation. Brain 2015;138:2020-33.
23. Jack CR Jr., Wiste HJ, Weigand SD, Therneau TM, Lowe VJ, Knopman DS, *et al*. Defining imaging biomarker cut points for brain aging and Alzheimer's disease. Alzheimers Dement 2017;13:205-16.
24. Lemoine L, Gillberg PG, Svedberg M, Stepanov V, Jia Z, Huang J, *et al*. Comparative binding properties of the tau PET tracers THK5117, THK5351, PBB3, and T807 in postmortem Alzheimer brains. Alzheimers Res Ther 2017;9:96.
25. Kikuchi A, Okamura N, Hasegawa T, Harada R, Watanuki S, Funaki Y, *et al*. *In vivo* visualization of tau deposits in corticobasal syndrome by 18F-THK5351 PET. Neurology 2016;87:2309-16.
26. Schöll M, Maass A, Mattsson N, Ashton NJ, Blennow K, Zetterberg H, *et al*. Biomarkers for tau pathology. Mol Cell Neurosci 2019;97:18-33.
27. Thal DR, Rüb U, Orantes M, Braak H. Phases of A beta-deposition in the human brain and its relevance for the development of AD. Neurology 2002;58:1791-800.
28. Ng KP, Pascoal TA, Mathotaarachchi S, Therriault J, Kang MS, Shin M, *et al*. Monoamine oxidase B inhibitor, selegiline, reduces 18 F-THK5351 uptake in the human brain. Alzheimers Res Ther 2017;9:25.
29. Harada R, Ishiki A, Kai H, Sato N, Furukawa K, Furumoto S, *et al*. Correlations of 18 F-THK5351 PET with postmortem burden of tau and astrogliosis in Alzheimer Disease. J Nucl Med 2018;59:671-4.